Journal of ELECTRONIC MATERIALS, Vol. 39, No. 12, 2010
DOI: 10.1007/s11664-010-1366-2

Magnetic Silver-Coated Ferrite Nanoparticles and Their Application in Thick Films

JIANGUO LIU,[1,3] BALING HUANG,[2] XIANGYOU LI,[1] PING LI,[2] and XIAOYAN ZENG[1]

1.—Wuhan National Laboratory for Optoelectronics, College of Optoelectronics Science and Engineering, Huazhong University of Science and Technology, Wuhan 430074, China. 2.—College of Chemistry and Chemical Engineering, Huazhong University of Science and Technology, Wuhan 430074, China. 3.—e-mail: ljg712@yahoo.com.cn

Magnetic silver-coated ferrite nanoparticles with 39.8% weight gain (relative to ferrite nanopowder coated by a silver layer) were synthesized by electroless deposition of silver on ferrite nanopowder. The mechanism of the electroless deposition was explored in terms of pretreatment, sensitization, activation, and the reduction of silver–ammonia complexes. Experiments showed that the optimal deposition conditions were a temperature of 50°C, pH value of 10 to 12, duration of 65 min with ethanol plus polyethylene glycol as additives, and ultrasonic vibration as a method of dispersing the nanoparticles. From transmission electron microscopy (TEM) images, it was observed that as-synthesized nanoparticles had a core–shell structure with a particle size of 35 nm to 90 nm and a shell thickness of 5 nm to 20 nm. X-ray diffraction (XRD) analysis confirmed that only ferrite and metallic silver were present in the product. Electrical resistance and magnetic hysteresis measurements demonstrated that the nanoparticles were both electrically conductive (volume electrical resistivity on the order of 10^{-4} Ω cm to 10^{-3} Ω cm when compressed to pressure of 2×10^{6} Pa) and possessed ferrimagnetic properties. After a thick-film paste, obtained with the nanoparticles as the functional phase, was directly written and sintered, scanning electron microscopy (SEM) analysis and electrical resistance measurements of conductive lines in the acquired array pattern showed that an electrically conductive network with some defects and cavities was formed, with a volume electrical resistivity of 1×10^{-4} Ω cm to 1×10^{-3} Ω cm.

Key words: Silver-coated ferrite nanoparticles, core–shell structure, electroless deposition, ferrimagnetism, thick-film paste

INTRODUCTION

With the rapid development of modern electronics, great progress has been made in the area of electronic materials over the past two decades. Silver (Ag), which is the most conductive bulk metal (electrical conductivity 6.62×10^{5} Siemens cm^{-1}) and can be fabricated as ultrafine (micrometer, submicron or nanometer) flakes or spherical powder, is widely used as a conductive phase in conductive adhesives, conductive inks, and thick-film pastes.[1–3] This has great potential to replace conventional tin/lead (Sn/Pb) solders in printed circuit boards (PCB), integrated circuits (IC), and chip packaging for environmental reasons.[4]

Ferrite (Fe_3O_4) is a nonmetallic material as well as a unique iron-containing compound that can be magnetized as a wave-absorbing material.[5,6] Generally, nonmetallic materials can be prepared as metal–nonmetallic composites through coprecipitation,[7] ball milling,[8] electroless deposition[9] or

(Received June 26, 2009; accepted August 13, 2010; published online September 14, 2010)

chemical reduction.[10] Among these methods, electroless deposition, based on autocatalytic reduction of metallic salt complexes, has many advantages, the most notable of which is uniform dispersion of the metallic coating.[11] Thus, metal–nonmetallic composites can acquire the properties of both metallic materials (e.g., conductivity and ductility) and nonmetallic materials (e.g., high melting point or magnetic properties). Furthermore, their anticorrosion, antiwear, and wetting capabilities can also be significantly improved.[12] It has been reported that Fe_3O_4-Ag composite nanoparticles have been applied in the biomedical field because of their ferrimagnetic properties.[13,14] As an electromagnetic material, it is anticipated that they can be used as the functional phase of thick-film pastes to fabricate, for example, thick-film inductors and anticounterfeit labels.

In this research, electroless deposition of Ag on the surface of Fe_3O_4 nanopowder was demonstrated, and the mechanism and processing conditions of the electroless deposition were explored. In addition, the properties of the as-synthesized Ag-coated Fe_3O_4 nanoparticles were investigated. Finally, preliminary tests involving the application of the nanoparticles as a functional filler phase in a thick-film paste were performed.

EXPERIMENTAL PROCEDURES

Materials

The employed materials included Fe_3O_4 nanopowder with a particle size of 10 nm to 50 nm (Shanghai Fritsch Instruments & Facilities Co., Ltd., China), Pb-free glass powder with a particle size of 5 μm to 40 μm (Taizhou Xinhai Special Materials Factory, China), and Ag nanopowder with a particle size of 5 nm to 100 nm (Shenzhen Zunye Nanomaterials Co., Ltd., China). Silver nitrate ($AgNO_3$), 25% ammonia ($NH_3{\cdot}H_2O$), 37% formaldehyde (HCHO), ethanol (EtOH), polyethylene glycol-400 (PEG), sodium hydroxide (NaOH), nitric acid (HNO_3), tin dichloride ($SnCl_2$), hydrochloric acid (HCl), carboxylmethyl cellulose (CMC), terpilenol, Span-85 (sorbitan trioleate), and tributyl citrate were purchased as analytical reagent (AR)-grade chemicals from Sinopharm Chemical Reagent. The raw materials were used as received without further purification. An alumina (Al_2O_3) substrate (0.5 mm thickness, 99.5 wt.% purity) was purchased from Suzhou Ruibang Advanced Ceramics Co., Ltd. (China).

Preparation of Ag-Coated Fe_3O_4 Nanoparticles

An electroless deposition bath composed of additives, with $AgNO_3$ (18 g to 35 g) as the main salt, ammonia (200 mL) as a complex agent, and HCHO as a reductant, was topped up to 1 L with deionized water. The loading of each additive was 5 wt.% (relative to the deposition bath). The pH value of the bath was adjusted using a NaOH aqueous solution (7 g L^{-1}) or 10% HNO_3 (the pH value was measured by a pH meter).

The as-purchased Fe_3O_4 nanopowder was treated with 5% to 10% HNO_3 for 3 min to 5 min at room temperature (25°C) under ultrasonic vibration (300 W power, 38 kHz frequency). They were then filtrated and washed with deionized water several times until neutral conditions (pH 7) were obtained.

The treated Fe_3O_4 nanopowder was sensitized in a $SnCl_2$ aqueous solution (15 g L^{-1}) for 5 min, then filtrated and washed with deionized water several times. Afterward, they were activated with an aqueous solution of $AgNO_3$ (30 g L^{-1}) for 3 min. The activated Fe_3O_4 nanopowder was filtrated and washed with deionized water several times.

The activated Fe_3O_4 nanopowder was added to the above-mentioned bath at different temperatures (25°C to 70°C). The electroless deposition was sustained for 10 min to 80 min with different stirring methods. Then it was filtrated, washed, and dried at 60°C under vacuum.

The above product was soaked in 30% HCl aqueous solution for 5 h. Next, it was washed and separated in a magnetic field to eliminate free Ag particles. Consequently, Ag-coated Fe_3O_4 nanoparticles were obtained.

Each of the electroless deposition procedures was repeated three times under identical conditions, and the results were averaged.

Preparation and Micropen Direct Writing of Thick-Film Paste

Under ultrasonic vibration and at room temperature, a thick-film paste was prepared with 80 wt.% Ag-coated Fe_3O_4 nanoparticles (39.8% weight gain) as the functional phase, 1 wt.% Pb-free glass powder as frit, and a 19 wt.% organic matrix (mainly including ethyl cellulose, terpilenol, Span-85, and tributyl citrate). The paste was directly written onto the alumina substrate by a micropen technique. The resulting array pattern was dried at 120°C for 20 min to evaporate solvents and sintered at temperatures ranging from 250°C to 550°C for 15 min. To test the volume electrical resistivity of the sintered paste, it was written into lines with dimensions of about 50 mm × 0.5 mm (length × width).

Measurements and Characterization

Transmission electron microscopy (TEM), x-ray diffraction (XRD), and scanning electron microscopy (SEM) were performed using a Tecnai G2 20 transmission electron microscope, an X' Pert PRO x-ray diffractometer, and a JSM5510LV scanning electron microscope, respectively. The fine structure of the Ag-coated Fe_3O_4 nanoparticles was observed by high-resolution TEM (HRTEM, Philips CM200).

The electroless deposition rate was expressed by the weight gain of the Fe_3O_4 nanopowder (measured

by an analytical balance at a precision of 0.0001 g). The weight gain was calculated using Eq. 1.

$$\text{Weight gain } (\%) = (W_2 - W_1)/W_1. \quad (1)$$

Here, W_2 denotes the total weight of the Fe_3O_4 nanopowder plus the Ag layer after purification, and W_1 denotes the weight of the Fe_3O_4 nanopowder coated by the Ag layer. As a result, the Ag content in the Ag-coated Fe_3O_4 nanoparticles can be calculated using Eq. 2.

$$\text{Ag content } (\%) = (W_2 - W_1)/W_2. \quad (2)$$

To test the volume electrical resistivity of the nanoparticles or nanopowder, a manual tablet-pressing machine (model L7690063; Shanghai Xiyu Electromechanical System Co., Ltd., China) with stainless-steel molds and pistons was employed to press the sample into a pellet. Under a pressure of 2×10^6 Pa and at room temperature, using a 5-cm-diameter mold and a 1-cm-diameter piston, 1.0 g of the sample was used to form a pellet with about 1 cm diameter and 0.1 cm thickness. Then the electrical resistance (R, Ω) between two surfaces of the pellet was measured by a direct-current (DC) four-probe method (Fig. 1). Two of the probes were used on each cross-section for passing an electrical current, while the other two were used for voltage measurement. Each probe was made of metallic tungsten and had a tip diameter of 25 μm. During the tests, each tip imposed about 3 N of force on the pellet to maintain good contact. The electrical resistance was determined by dividing the measured voltage by the current.

The electrical resistivity (ρ, Ω cm) of the nanoparticles or nanopowder was calculated using Eq. 3.

$$\rho = RA/H = \pi RD^2/4H. \quad (3)$$

Here, A, H, and D denote the cross-sectional area (cm^2), thickness (about 0.1 cm), and diameter (about 1 cm) of the pellet, respectively. The electrical resistance, thickness, and diameter of the pellet were measured separately three times for each specimen, and the results were averaged. Five specimens were tested.

The electrical resistance (R, Ω) of a line made using the sintered paste was also measured by the above DC four-probe method. Here the outer two tungsten probes (40.0 mm apart) were used for passing an electrical current, while the inner two (20.0 mm apart) were employed for the voltage measurement. The other procedures were the same as those described above. The electrical resistivity (ρ, Ω cm) was calculated using Eq. 4.

$$\rho = RA/L = RHw/L. \quad (4)$$

Here, the cross-sectional area (A, cm^2) of the line is equal to its thickness (H, cm) multiplied by its width (w, cm), and L denotes the length (cm) of the line. The thickness and width (profile) of the line were measured by a surface probe profilometer (model KLA-Tencor P16+). The electrical resistance, thickness, width, and length of the line were separately measured three times for each specimen, and the results were averaged. Five specimens were tested.

To study the magnetic properties of the nanoparticles or nanopowder, under 2×10^6 Pa pressure, using a 4-cm-diameter mold and a 0.3-cm-diameter piston, 0.5 g of the sample was pressed by the above-mentioned tablet-pressing machine to form a sample cylinder with about 0.3 cm diameter and 0.5 cm height. At room temperature, the sample cylinder was placed in the magnetic field of a Lake Shore 7410 vibrating sample magnetometer. The magnetic field changed continuously at the rate of 500 Oe/min from 0 Oe to 10 kOe, then from 10 kOe to 0 Oe, then from 0 Oe to −10 kOe, and then from −10 kOe to 0 kOe. At the same time, the magnetization of the sample was recorded to acquire a magnetic hysteresis loop. The saturation magnetization and coercivity of the sample were obtained from the magnetic hysteresis loop. The magnetization of each sample was separately measured three times, and the results were averaged. Five samples were tested.

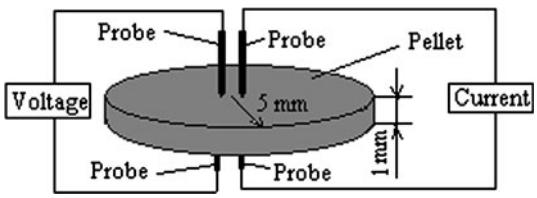

Fig. 1. Schematic diagram of the DC four-probe method for measuring the volume electrical resistivity of the sample pellets.

RESULTS AND DISCUSSION

Mechanism of Electroless Deposition of Ag on the Surface of Fe_3O_4 Nanopowder

Fe_3O_4 nanopowder is nonmetallic. The electroless deposition of metal includes processes such as pretreatment, sensitization, and activation.[15–19]

Pretreatment is used to eliminate contaminants and roughen the surface to decrease the surface energy.

During sensitization, the surface of the Fe_3O_4 nanopowder adsorbs Sn^{2+} ions from the $SnCl_2$ aqueous solution. Then, during activation, these Sn^{2+} ions are able to reduce Ag^+ ions to yield metallic Ag atoms according to Eq. 5.

$$Sn^{2+} + 2Ag^+ = 2Ag + Sn^{4+} \quad (5)$$

For further electroless deposition, the Ag atoms act as active centers and catalyze the following reaction (Eq. 6).

$$2Ag(NH_3)_2OH + HCHO = 2Ag + HCOOH + 4NH_3 + H_2O \quad (6)$$

As the Ag atoms precipitate, more of the Fe_3O_4 particle surface is covered until it is coated thoroughly. If some of the particle surfaces are uncovered or not coated thoroughly, the particles dissolve in the HCl aqueous solution (Eq. 7). Afterwards, the free Ag particles are removed by a magnetic field. During electroless deposition, it is very difficult for large quantities of Ag atoms and Fe_3O_4 molecules to dope and/or diffuse into each other.[20–22] Therefore, it can be inferred that the as-synthesized Fe_3O_4-Ag nanoparticles have a core–shell structure with Fe_3O_4 as the core and Ag as the shell. This was verified by HRTEM.

$$Fe_3O_4 + 8HCl = FeCl_2 + 2FeCl_3 + 4H_2O \quad (7)$$

The above processes are summarized as follows.[23,24]

Fe_3O_4 nanopowder
→ Pretreatment → Sensitization
→ Activation → Electroless deposition of Ag
→ Ag-coated Fe_3O_4 nanoparticles

Factors Influencing the Electroless Deposition of Ag

The experiments revealed that deposition temperature, pH value, additives, duration, and stirring method were the main factors affecting the electroless deposition of Ag.

The effect of temperature on the electroless deposition was significant. The higher the temperature, the higher the electroless deposition rate (Fig. 2). However, at high temperatures (>55°C), the electroless deposition solution was less stable. Additionally, it was observed that the quality of the deposited layer was poor and resulted in peeling and craze cracking. If the temperature was too high, the electroless deposition solution would decompose. For temperatures between 45°C and 55°C, the rate was moderate, and no peeling or craze cracking was observed in the deposited layer. Below this temperature, the rate was too small to generate a good Ag layer within 90 min.

Although the reducibility of HCHO was poor in acidic solution, it became stronger with increasing pH value in the deposition bath. It was found that the electroless deposition rate was optimal for pH values ranging from 10 to 12. When the pH value was larger than 12, decomposition of HCHO was inevitable, and the quality of the Ag layer was poor. During the electroless deposition, the pH value decreased gradually (Fig. 3). This was due to the continual generation of formic acid (HCOOH) with the oxidization of HCHO. Thus, it was necessary to control the pH value by dropping NaOH (7 g L^{-1}).

Additives were also found to play an important role in the electroless deposition. They were able to adsorb and/or disperse uniformly on the interface between the Fe_3O_4 nanopowder and the solution, and to decrease the surface energy of the nanoparticles. Common additives include synthetic polymers, natural polymers, and small molecular compounds. In this work, additives (or their combinations) such as PEG, CMC, and EtOH were explored. As shown in Fig. 4, it was found that all of the combinative additives (i.e., EtOH + CMC, EtOH + PEG, CMC + PEG, and EtOH + CMC + PEG) had an effect on the electroless deposition rate. Among those, the effect of the combination of EtOH + PEG was the largest. After 60 min electroless deposition, the weight gain increased to about 40%. As a result, this combination was selected as the additive for the electroless deposition.

The effect of reaction duration on weight gain is illustrated in Fig. 5. The weight gain initially increased linearly with duration and then plateaued

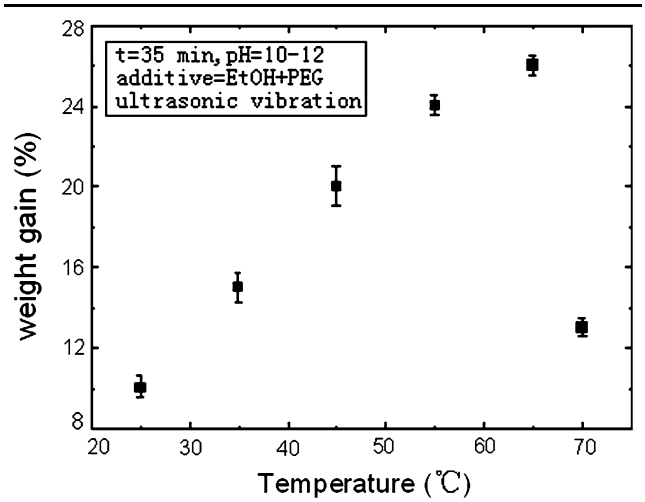

Fig. 2. Effect of temperature on weight gain.

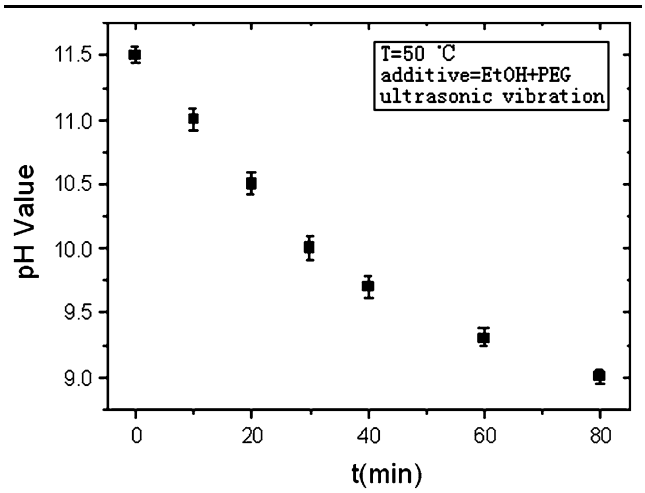

Fig. 3. Relationship between reaction duration (*t*) and pH value.

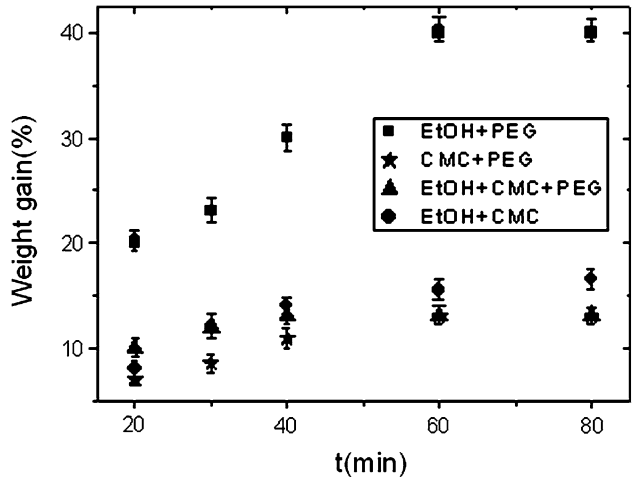

Fig. 4. Effect of combinative additives on weight gain.

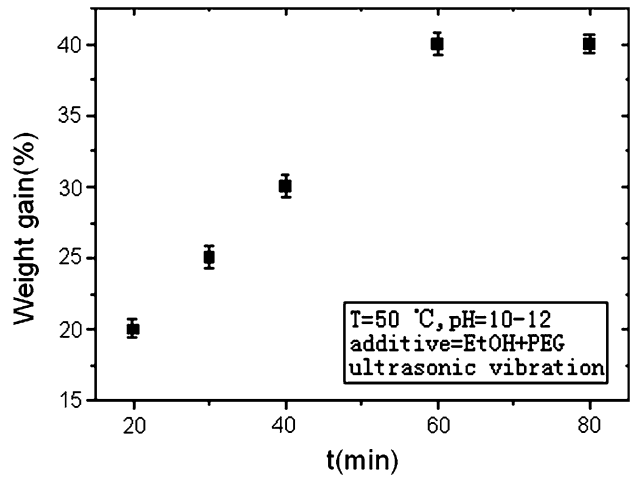

Fig. 5. Effect of reaction duration (t) on weight gain.

in the range of 50 min to 60 min. Beyond this range, the change in weight gain was very slow, so the duration of the electroless deposition was chosen to be about 65 min.

Different stirring methods were observed to affect the dispersion of the Fe_3O_4 nanopowder in the bath. Uniform dispersion allowed for greater contact area of the Fe_3O_4 nanoparticles in the bath. Thus, the weight gain was greater for better stirring methods. Three stirring methods (i.e., mechanical stirring, ultrasonic vibration, and mechanical stirring plus ultrasonic vibration) were adopted in this experiment. The effects of the stirring methods on weight gain for a given temperature, duration, pH value, and additive are listed in Table I. It was found that the weight gain was the highest (40 ± 1.6%) when using ultrasonic vibration. Thus, ultrasonic vibration was chosen for subsequent experiments.

Thus, the optimal deposition conditions were a temperature of 50°C, pH of 10 to 12 with EtOH plus PEG as additives, duration of 65 min, and ultrasonic vibration as the dispersing method. Under these conditions, Ag-coated Fe_3O_4 nanoparticles with the highest weight gain (about 40%) were produced, and the Ag content in the nanoparticles was calculated to be about 30 wt.% (28.6 wt.%). In this case, the utilized rate of the raw materials (Fe_3O_4 and $AgNO_3$) was optimal. When Ag-coated Fe_3O_4 nanoparticles with lower Ag content (e.g., ≤25 wt.%) were synthesized, more of the Fe_3O_4 nanopowder was wasted because they could not be encapsulated thoroughly and would be dissolved in the HCl aqueous solution. Thus, the Ag-coated Fe_3O_4 nanoparticles with lower Ag content were not explored further.

Table I. Effect of stirring method on weight gain

Stirring Method	Weight Gain (%)
Mechanical stirring (0 rpm to 6000 rpm)	31.0 ± 2.1
Ultrasonic vibration (300 W power, 38 kHz frequency)	40.0 ± 1.6
Mechanical stirring plus ultrasonic vibration	37.5 ± 1.3

TEM and XRD Analyses of Fe_3O_4 Nanopowder and Ag-Coated Fe_3O_4 Nanoparticles

TEM (Fig. 6a) of the Fe_3O_4 nanopowder showed that the initial particle size was about 10 nm to 50 nm. After the electroless deposition of Ag (39.8% weight gain), the particles became larger, with a size of 35 nm to 90 nm (Fig. 6b). Using HRTEM images of the Ag-coated Fe_3O_4 nanoparticles (Fig. 6c, d), their fine structure was studied. Cores and shells were clearly observed in the nanoparticles, with the shell thickness ranging from 5 nm to 20 nm. Therefore, the as-synthesized Ag-Fe_3O_4 nanoparticles had a core–shell structure. Additionally, the nanoparticles were found to lightly agglomerate, which probably resulted from agglomeration of the as-purchased Fe_3O_4 nanopowder. During the electroless deposition, the agglomerated particles behaved as a single core.

An XRD spectrum of the Ag-coated Fe_3O_4 nanoparticles is shown in Fig. 7, where diffraction peaks of the Fe_3O_4 and Ag phases were observed. However, no other diffraction peaks were present. This indicated that no other phases, e.g., $Ag_x(Fe_3O_4)_{1-x}$ ($0 < x < 1$), were present in the Ag-coated Fe_3O_4 nanoparticles.[20,21] This was consistent with the observation of a core–shell structure in the nanoparticles.

Electrical Conductivity of Ag-Coated Fe_3O_4 Nanoparticles

It is known that at, room temperature, the volume electrical resistivity of bulk Ag is about 1.6×10^{-6} Ω cm ($\rho_{Ag} = 1.6 \times 10^{-6}$ Ω cm) and that of bulk ferrite is 10^8–10^{12} Ω cm (average

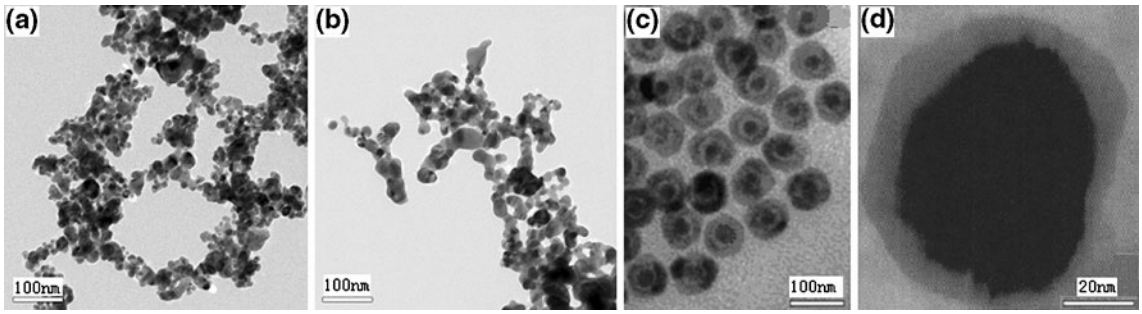

Fig. 6. TEM (a and b) and HRTEM (c and d) images of Fe_3O_4 nanopowder (a) and Ag-coated Fe_3O_4 nanoparticles (b–d, 39.8% weight gain).

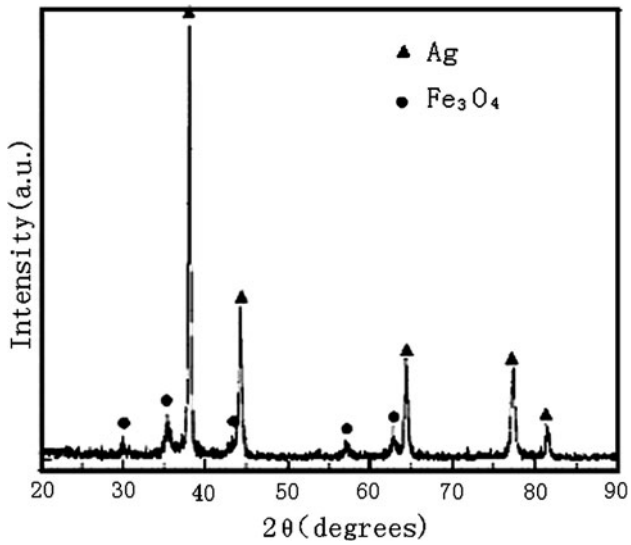

Fig. 7. XRD spectrum of Ag-coated Fe_3O_4 nanoparticles (39.8% weight gain).

$\rho_{ferrite} = 10^{10}$ Ω cm).[21] We can calculate the volume electrical resistivity (ρ) of a resistor formed by bulk silver and ferrite according to the rule of mixtures. In the case of serial connection, the resistivity (ρ_{serial}) of the resistor can be expressed using Eq. 8.

$$\rho_{serial} = x\rho_{Ag} + (1-x)\rho_{ferrite}. \quad (8)$$

Meanwhile, in the case of a parallel connection, the resistivity ($\rho_{parallel}$) of the resistor can be expressed using Eq. 9.

$$\rho_{parallel} = [x\rho_A \times (1-x)\rho_{ferrite}]/[x\rho_{Ag} + (1-x)\rho_{ferrite}]. \quad (9)$$

Here, x denotes the volume fraction of Ag in the resistor, and $(1-x)$ is the volume fraction of ferrite.

The weight content of Ag in the as-synthesized nanoparticles with 39.8% weight gain was calculated to be 28.5% using Eq. 2. Because the densities of bulk Ag and ferrite are about 10.5 g cm^{-3} and 5.2 g cm^{-3}, respectively,[21] the volume fraction of Ag in the nanoparticles was estimated to be 16.5% (i.e., x = 16.5%). Thus, $\rho_{serial} \approx 8.4 \times 10^9$ Ω cm and $\rho_{parallel} \approx 2.6 \times 10^{-7}$ Ω cm.

The measured electrical resistance and calculated volume electrical resistivity of the Ag-coated Fe_3O_4 nanoparticles (39.8% weight gain, compressed by 2×10^6 Pa of pressure) are listed in Table II. It can be seen that the resistivity was on the order of 10^{-3}–10^{-4} Ω cm, which was higher than that of bulk Ag (1.6×10^{-6} Ω cm), much less than that of bulk ferrite, and between ρ_{serial} and $\rho_{parallel}$. It is obvious that the measured resistivity of the Ag-coated Fe_3O_4 nanoparticles is not in accordance with the value calculated from the serial or parallel connection models. An appropriate model to calculate the resistivity of the Ag-coated Fe_3O_4 nanoparticles needs to be established in the future. As a comparison, when 28.5 wt.% Ag nanopowder and 71.5 wt.% Fe_3O_4 nanopowder were blended thoroughly to generate a mixture and then compressed at 2×10^6 Pa to form a pellet, the volume electrical resistivity was measured to be about 30 Ω cm to 60 Ω cm, which was much higher

Table II. Volume resistivity of Ag-coated Fe_3O_4 nanoparticles (39.8% weight gain, compressed at 2×10^6 Pa pressure)

Samples	Measured Resistance (Ω)	Diameter of Sample Pellet (cm)	Thickness of Sample Pellet (cm)	Volume Resistivity ($\times 10^{-4}$ Ω cm)
1	1.0×10^{-4}	0.99	0.094	8.3
2	1.5×10^{-4}	0.98	0.097	11.5
3	6.6×10^{-5}	1.0	0.093	5.6
4	1.6×10^{-4}	1.0	0.095	13.4
5	1.5×10^{-5}	0.99	0.098	1.2

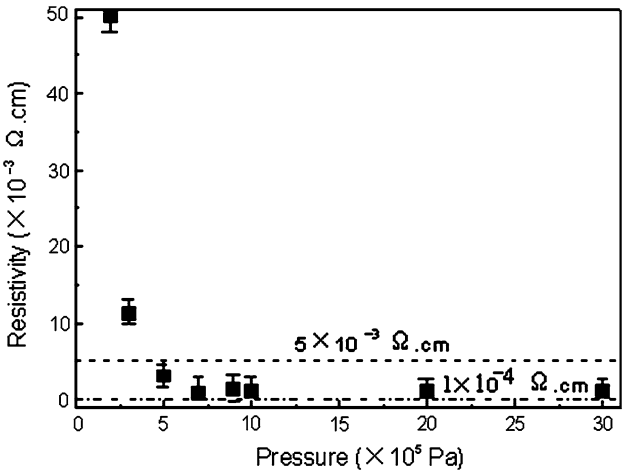

Fig. 8. Effect of pressure on the volume electrical resistivity of Ag-coated Fe_3O_4 nanoparticles (39.8% weight gain).

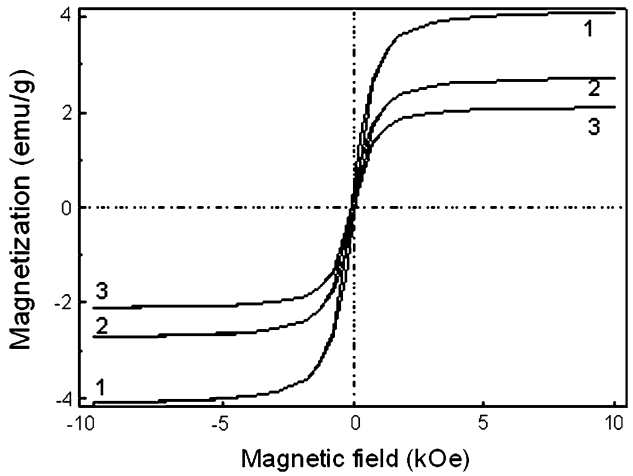

Fig. 9. Magnetic hysteresis loops for: (1) Fe_3O_4 nanopowder, (2) mixture of 71.5 wt.% Fe_3O_4 nanopowder and 28.5 wt.% Ag nanopowder, and (3) Ag-coated Fe_3O_4 nanoparticles (39.8% weight gain).

than that of the Ag-coated Fe_3O_4 nanoparticles (39.8% weight gain).

Further tests showed that, under the same pressure, when increasing the weight content of silver in the mixture consisting of silver and Fe_3O_4 nanopowder, the electrical resistivity decreased. When the content approached 100 wt.%, the resistivity of the mixture was close to that of the Ag-coated Fe_3O_4 nanoparticles (39.8% weight gain). Thus, the Ag-coated Fe_3O_4 nanoparticles were good conductors. The Ag layer on the surface formed an electrically conductive network and enhanced the electrical conductibility. Additionally, the resistance to oxidation of the nanoparticles was also improved.[14]

The experiments also showed that the pressure used when preparing the sample pellets had an effect on the electrical resistivity of the Ag-coated Fe_3O_4 nanoparticles (Fig. 8). For low pressures (0 Pa to 10^5 Pa), the resistivity reduced significantly with increasing pressure. However, when the pressure was larger than 5×10^5 Pa, the resistivity varied only slightly and was on the order of 10^{-4} Ω cm to 10^{-3} Ω cm. This indicated that, under enough pressure, the contact between the nanoparticles was sufficient, so the resistivity did not change further. Therefore, all of the above sample pellets were prepared under a pressure of 2×10^6 Pa.

Magnetic Properties of Fe_3O_4 Nanopowder and Ag-Coated Fe_3O_4 Nanoparticles

It is known that metallic Ag is not magnetic, so the saturation magnetization of Ag nanopowder is zero. Ferrite is a soft magnetic material, and the saturation magnetization of its nanopowder was measured to be 4.10 ± 0.12 emu/g. According to the rule of mixtures, we calculated the saturation magnetization (M) of the Ag-coated Fe_3O_4 nanoparticles with different volume fraction of Ag using Eq. 10.

$$M = xM_{\mathrm{Ag}} + (1 - x)M_{\mathrm{ferrite}}. \quad (10)$$

Here, x is as defined above, M_{Ag} denotes the saturation magnetization of Ag nanoparticles ($M_{\mathrm{Ag}} = 0$), and M_{ferrite} denotes the saturation magnetization of the Fe_3O_4 nanopowder ($M_{\mathrm{ferrite}} = 4.10$ emu/g). Therefore, $M = (1 - x)M_{\mathrm{ferrite}} = 4.10(1 - x)$.

If $x = 16.5\%$, then $M = 3.42$ (emu/g), i.e., according to this rule, the saturation magnetization (M) of the Ag-coated Fe_3O_4 nanoparticles with 39.8% weight gain was calculated to be 3.42 emu/g.

However, the testing results showed that the saturation magnetization of the Ag-coated Fe_3O_4 nanoparticles with 39.8% weight gain was only 2.10 ± 0.05 emu/g, which was approximately half of that of the Fe_3O_4 nanopowder and was significantly different from the calculated value.

As a comparison, we measured the saturation magnetization of a mixture consisting of 71.5 wt.% Fe_3O_4 nanopowder and 28.5 wt.% silver nanopowder to be 2.72 ± 0.08 emu/g, which was significantly different from that of the Ag-coated Fe_3O_4 nanoparticles (39.8% weight gain). This difference may be due to a stronger magnetic shielding capability resulting from thorough encapsulation of the silver layer on the Fe_3O_4 nanocore.

Magnetic hysteresis loops of the Fe_3O_4 nanopowder, the mixture consisting of 71.5 wt.% Fe_3O_4 nanopowder and 28.5 wt.% silver nanopowder, and the Ag-coated Fe_3O_4 nanoparticles with 39.8% weight gain are shown in Fig. 9, where it can be seen that the shapes of all the magnetic hysteresis loops are similar. In addition, due to the existence of apparent coercivity, the Ag-coated Fe_3O_4 nanoparticles exhibited typical ferrimagnetic behavior.

The experiments showed that the pressure used when preparing the sample cylinder had no effect on the magnetic properties when the pressure was less than 10^9 Pa.

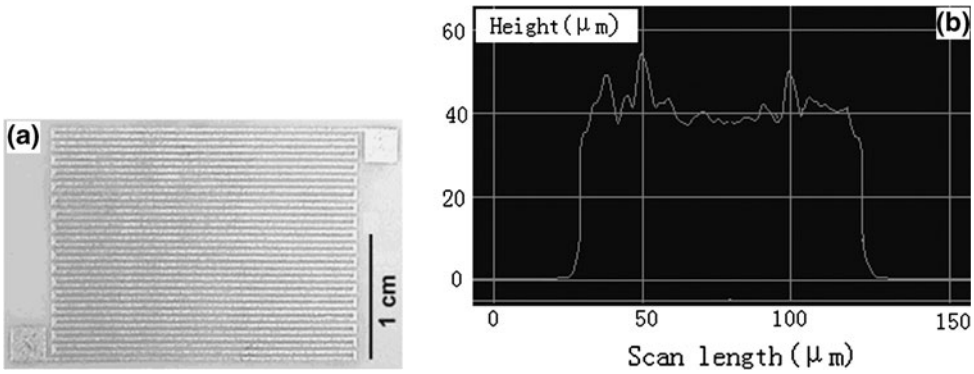

Fig. 10. Direct-writing array pattern (a) and cross-sectional profile (b) of a line in the array pattern.

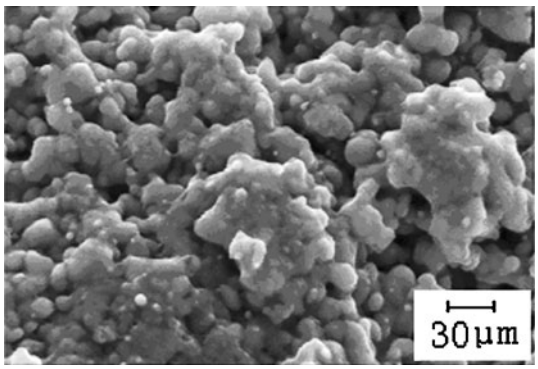

Fig. 11. SEM photograph of an array pattern resulting from direct writing and sintering of a thick-film paste.

Thick-Film Paste

After a thick-film paste, obtained with the Ag-coated Fe_3O_4 nanoparticles as the functional phase, was directly written and sintered, an array pattern (Fig. 10a) was acquired. The cross-sectional profile of a line in the array pattern is shown in Fig. 10b. It could be seen that the thickness and width of the line were about 40 μm and 100 μm, respectively. The micromorphology (Fig. 11) of the array pattern was analyzed by SEM. It was found that an electrically conductive network of sintered nanoparticles was formed. However, the network was not perfectly regular but had defects and cavities. Measurements showed that its electrical resistivity was 10^{-4} Ω cm to 10^{-3} Ω cm, which was higher than that of an electrically conductive paste with pure silver nanoparticles as the functional phase (about 10^{-6} Ω cm to 10^{-5} Ω cm).[25] This higher electrical resistivity is probably due to the presence of the defects and cavities. Further investigation is necessary to obtain better electrical conductibility. As an electrically conductive material, the Ag-coated Fe_3O_4 nanoparticles preserve the electrically conductive characteristics of metallic silver to some extent, but their potential applications in other areas (e.g., thick-film inductors) need to be developed in the near future.

CONCLUSIONS

Electroless deposition of Ag on the surface of Fe_3O_4 nanopowder was realized. The deposition process included pretreatment, sensitization, activation, and the reduction of a silver–ammonia complex. The effects of temperature and pH value on the electroless deposition and the effects of additives, deposition duration, and stirring method on the weight gain were explored. The optimal process conditions for the electroless deposition were a temperature of 50°C and pH value of 10 to 12, with EtOH plus PEG as additives, deposition duration of 65 min, and ultrasonic vibration as a dispersing method. Under the optimal conditions, Ag-coated Fe_3O_4 nanoparticles with the highest weight gain (39.8%) were synthesized. TEM images showed that the size of the as-synthesized nanoparticles with light agglomeration ranged from 35 nm to 90 nm, and HRTEM images showed that they had a core–shell structure with a Ag shell thickness of 5 nm to 20 nm. XRD analysis confirmed that only Fe_3O_4 and Ag phases were present in the product. Electrical measurements showed that the volume electrical resistivity of the nanoparticles was on the order of 10^{-4} Ω cm to 10^{-3} Ω cm (for pellets formed by compression at pressure of 2×10^6 Pa). The magnetic hysteresis loop revealed the ferrimagnetic behavior of the nanoparticles. Preliminary studies on an application of the nanoparticles as a functional filler phase in thick-film paste were performed.

ACKNOWLEDGEMENTS

The project was supported by the National Natural Science Foundation of China (Grant No. 60806035). We thank the Analytical and Testing Center of Huazhong University of Science and Technology for performing TEM, SEM and XRD testing.

REFERENCES

1. S.A. Ketkar, G.G. Umarji, G.J. Phatak, J.D. Ambekar, U.P. Mulik, and D.P. Amalnerkar, *Mater. Chem. Phys.* 132, 145 (2006).

2. S.H. Park, D.S. Seo, and J.K. Lee, *Colloids Surf. A* 313–314, 197 (2008).
3. A.S. Grijalva, R.H. Urbina, J.F.R. Silva, M.A. Borja, F.F.C. Barraza, and A.P. Amarillas, *Mater. Res. Bull.* 43, 90 (2008).
4. K.J. Lee, B.H. Jun, J. Choi, Y. Lee, II, J. Joung, and Y.S. Oh, *Nanotechnology* 18, 335601 (2007).
5. Y.H. Zheng, Y. Cheng, F. Bao, and Y.S. Wang, *Mater. Res. Bull.* 41, 525 (2006).
6. C.Y. Wang, G.M. Zhu, Z.Y. Chen, and Z.G. Lin, *Mater. Res. Bull.* 37, 2525 (2002).
7. G.J. Li, X.X. Huang, and J.K. Guo, *Mater. Res. Bull.* 36, 1307 (2001).
8. T. Puclin and W.A. Kaczmarek, *J. Alloys Compd.* 266, 283 (1998).
9. G.W. Wen, Z.X. Guo, and C.K.L. Davies, *Scripta Mater.* 43, 307 (2000).
10. H.J. Hwang, M. Toriyama, T. Sekino, and K. Niihara, *J. Eur. Ceram. Soc.* 18, 2193 (1998).
11. W.X. Shi, J. Yang, and T.J. Wang, *J. Phys. Chem.* 17, 507 (2001).
12. S.Y. Chang, J.H. Lin, S.J. Lin, and T.Z. Kattamis, *Metall. Mater. Trans. A* 30, 1119 (1999).
13. D.P. Tang, R. Yuan, and Y.Q. Chai, *J. Phys. Chem. B* 110, 11640 (2006).
14. X.Y. Guo, Y.N. Wang, L.G. Gu, Y.F. He, C.X. Zhang, Z.M. Tang, and Z.H. Lu, *Chem. J. Chin. Univ.* 27, 1725 (2006) (in Chinese).
15. L.M. Ang, T.S.A. Hor, G.Q. Xu, C.H. Tung, S.P. Zhao, and J.L.S. Wang, *Carbon* 38, 363 (2000).
16. S.L. Brandow, M.S. Chen, and T. Wang, *J. Electrochem. Soc.* 144, 3425 (1997).
17. Y. Kobayashi, V. Salgueirino-Maceira, and L.M. Liz-Marzan, *Chem. Mater.* 13, 1630 (2001).
18. M.V. Ten Kortenaar, J.J.M. De Goeij, Z.I. Kolar, G. Frens, P.J. Lusse, M.R. Zuiddam, and E. Van Der Drift, *J. Electrochem. Soc.* 148, 28 (2001).
19. H. Chang, C.H. Pitt, and G.B. Alexander, *J. Mater. Sci.* 28, 5207 (1993).
20. X.H. Hu, M.H. Xu, X.G. Cui, and S.Y. Zhang, *Solid State Commun.* 142, 595 (2007).
21. J.H. Hsu, S.Y. Chen, W.M. Chang, and C.R. Chang, *J. Magn. Magn. Mater.* 272–276, 1772 (2004).
22. Y. Kimishima, W. Yamada, M. Uehara, T. Asaka, K. Kimoto, and Y. Matsui, *Mater. Sci. Eng. B* 138, 69 (2007).
23. S.G. Warrier and R.Y. Lin, *J. Mater. Sci.* 28, 4868 (1993).
24. L. Zhang, Y.H. Dou, and H.C. Gu, *J. Colloid Interface Sci.* 297, 660 (2006).
25. H.H. Lee, K.S. Chou, and Z.W. Shin, *Int. J. Adhes. Adhes.* 25, 437 (2005).